VII International Conference on Computational Methods in Marine Engineering
MARINE 2017
M. Visonneau, P. Queutey and D. Le Touzé (Eds)

SYSTEMATIC ANALYSIS OF MESH AND MESHLESS CFD METHODS FOR WATER IMPACT PROBLEMS

LUCA BONFIGLIO*, STEFANO GAGGERO†, ALDO PAPETTI†, GIULIANO VERNENGO† AND DIEGO VILLA†

*MIT Sea Grant College Program
Massachusetts Institute of Technology
Cambridge, 02139-4307, MA, USA
e-mail: bonfi@mit.edu

† Dept. of Electric, Electronic and
Telecomunication Engineering and Naval Architecture (DITEN)
University of Genova
Genova, 16145, Italy
e-mail: stefano.gaggero@unige.it, giuliano.vernengo@unige.it, diego.villa@unige.it

Key words: Slamming, Violent Impact Hydrodynamics, Impact Forces, Free Surface Deformation, Unsteady Reynolds Averaged Navier Stokes (URANS), Smoothed Particle Hydrodynamics (SPH)

Abstract. Two types of numerical simulations for the hydrodynamic solution of water entry problems are performed and systematically compared in order to highlight their peculiarities: a viscous Unsteady Reynolds Averaged Navier Stokes (URANS) based on Volume of Fluid (VoF) approach and a meshless Smooth Particle Hydrodynamics (SPH) solver. In both cases open-source software have been chosen. The numerical solutions from the two proposed CFD methods are verified against experimental measurements. The systematic analysis is performed considering a prescribed motion of the wedge aiming to a better understanding of the effect of the model set-up on the prediction of both local and global field variables. Even if a both codes shows a high ability to capture the global physics of the problem, due to the strongly non-linear dynamic of the body-flow interactions involved in impact problems, the local pressure peaks can be hardly predicted if the numerical method is not suitably tuned for the specific problem. Finally the two approaches are performed also for a free falling simulation, comparing the numerical predictions to the available experimental drop tests results.

1 INTRODUCTION

Due to the strongly non-linear nature of the involved phenomena, impact hydrodynamics of falling bodies is a good test case to assess the capabilities of Computational Fluid Dynamics (CFD) solvers. Also, this is a very interesting problem in naval architecture since it is directly related to seakeeping, slamming loads and even more complex coupled analysis such as those

for ship springing and whipping generally resulting in various types of structural damages. The simpler experiment for such a class of problem consists of a drop test on symmetric or asymmetric bodies, such as wedges, cylinders or ship-like sections, usually meeting the bi-dimensional simplification. The first theoretic formulations belong to Von Karman [1] and Wagner [2] valid for small local wedge angles. Later Dobrovol'skaya [3] provides the so-called *similar solution* for wedges forced to impact the free surface at constant speed that needs to be solved numerically since given in implict form. More recently, a great impulse to the numeric solution of the problem has been given by Faltinsen who develops solutions based on different approaches such as non-linear Boundary Element Method with a jet model (see for instance [4] and [5]) or matched asymptotic expansions technique [6]. Considering other numerical techniques, mesh-based Unsteady Reynolds Averaged Navier-Stokes (URANS) and mesh-less Smoothed Particle Hydrodynamics (SPH) methods are gaining higher levels of maturity both as formulations and from the hardware-related side to be considered for both research and practical applications [7]. However there are still some open questions for example on the effects of the model set-up on the accuracy and stability of the searched solution and on the possibility to generalize the obtained results. Many examples of solutions of the wedge impact problem using both methods can be found in literature (see among the other [9], [8], [10], [11], [12], [13] and [14]). Some preliminary analysis on the influence of some model parameters on the solution of wedges impact have also been recently given in [15] and [16]. The proposed numeric study aims exactly at a better understanding of the effects of the simulation set-up on the hydrodynamics solution of impact-related problems. This is achieved by a systematic analysis of some the most relevant model parameters of both CFD methods; both the local pressures and the global forces on the body are extracted from the simulations and compared to available experimental measurements. The two methods, namely the URANS and the SPH are briefly described and results are shown separately. A final comparison among the two methods is performed and discussed in the light of the different formulations.

2 SELECTED TEST CASE FOR VALIDATION

All the computations presented in the study refer to the symmetric wedge tested by [17] with wedge angle $\alpha = 25°$. The test reproduced in the systematic numeric analysis of the two CFD methods corresponds to a free falling from an initial height of $h_{Drop} = 1.3m$ with the mass of the wedge equal to $m_W = 94kg$. In order to speed-up the analysis, all the computations have been performed using the vertical displacements of the wedge measured during the drop test and provided in the referenced paper; hence, the simulations have been ran for a reduced range of time with respect to the physical duration of the experiments, focusing on the impact of the wedge into the water and excluding part of the initial falling and of the tail of the drop test. The tested wedge have been equipped with twelve pressure transducer uniformly spaced along the face of the wedge itself as schematically shown in Figure 1. Due to the experimental set-up this test can be considered as bi-dimensional.

3 DESCRIPTION OF THE NUMERICAL METHODS

Two codes have been explored to tackle the wedge impact problem. The first is a mesh-based code which solves the viscous flow motion by means of the classical Finite Volume approximation

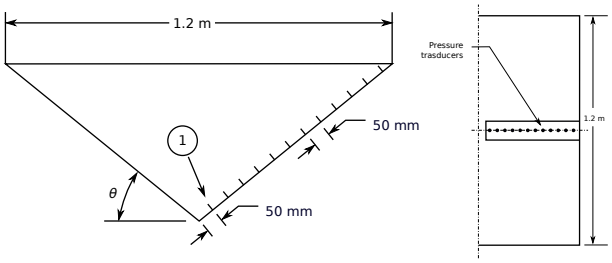

Figure 1: Wedge front and top view showing the dimensions and the pressure transducer locations [17].

(FV). The second one is a mesh-free code based on the discretization of the fluid flow by means of smooth discrete particle (SPH). Both codes have the ability to solve the 6-DoF dynamic (for the present case only 1-DoF is considered) or to constrain the wedge to move following a prescribed path. The second approach has been preferred to analyze the solver parameters in terms of force and pressure results neglecting their influence on the wedge motion. The selected path has been extracted by the original paper [17]. After the selection of the proper model set-up the free falling simulation has been compared with the experimental results.

3.1 MESH-BASED APPROACH: URANS

An open-source mesh-based viscous code has been used in the present paper to be compared with the mesh-free approach. The viscous code is a part of the OpenFOAM framework which is a general purpose CFD solver based on the finite volume approximation. A modified version of the classical Navier-Stokes flow system of equations in its unsteady form is solved to tackle the wedge entrance problem. Indeed, this problem is complicated by the presence of a highly distorted free surface.
Numerically, the presence of the two fluids can be taken into account in different ways. Here it is exploited by means of the Volume of Fluid (VoF) approach. This method is based on the flow-mixture theory which add a new scalar field (α) that represents the amount of liquid (or gas) in any point inside the domain. Consequently all the fluid properties will be further defined by a weighted average of the two considered fluids properties (air and water). The subscript l,g,m respectively stand for liquid, gas and mixture. They are summarized in Eq. (1).

$$\begin{aligned} \rho_m(x,t) &= \rho_l \cdot \alpha + \rho_g \cdot (1-\alpha) \\ \mu_m(x,t) &= \mu_l \cdot \alpha + \mu_g \cdot (1-\alpha) \end{aligned} \tag{1}$$

The α field is further transported in time through a purely convective equation, which takes into account the mass conservation of each phase of the mixture considering their immiscible nature. The new system of equations, reported in Eq. (2), presents a similar form of the starting N-S ones referred to the whole mixture.

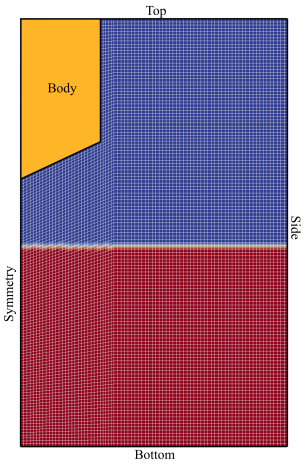

Figure 2: Multi-block structured mesh arrangement (coarser one)

$$\begin{cases} \nabla \cdot U_m = 0 \\ \dfrac{\partial U_m}{\partial t} + \nabla(U_m \otimes U_m) = -\dfrac{\nabla p_m}{\rho_m} + \nu_m \nabla^2(U_m) \\ \dfrac{\partial \alpha}{\partial t} + \nabla(U\alpha) = 0 \end{cases} \tag{2}$$

Numerically the equations are discretized using a first order time scheme and a second order accurate schemes for spatial derivatives. In particular the convective equation of the Volume of Fluid is solved by means of the *ad-hoc* developed Predictor-Corrector Semi-Implicit Multidimensional Universal Limiter for Explicit Solution (MULES) scheme: it was properly designed to solve the phase equation ensuring the boundedness of the void fraction, increasing also the time stability (i.e. allowing for Courant numbers higher than 1) compared to the purely explicit version. The proposed schemes have been selected as a good compromise between accuracy and numerical stability of the solver. Regarding the choice of the order for time derivatives approximation, a preliminary analysis, not fully reported here for shortness, has been performed. It demonstrated that the simulation adopting the second order scheme provided quite similar results, both in terms of global force and pressure signals on the wedge, with respect to the first order approximation. Simulations with second order schemes, however, suffered of a lower stability and numerical noise which definitely headed towards the first order approximation.
Thanks to nature of the performed tests, the problem was simplified to a 2-D representation of the wedge with purely bi-dimensional flow features. This simplification (widely adopted for this type of problems [4]) reduced of several order the computational effort required to solve the flow field without any significant loss of reliability compared to almost 2-D measurements. The mesh has been arranged by using of the OpenFOAM utility *blockMesh*, which generates structured multi-block meshes. An example (with the coarser mesh) is reported in figure 2. Due to the body-fitted structure of the mesh (i.e. no overlapping) the motion of the wedge was simply achieved by a rigid translation of the entire computational domain. This simple approach presumes an infinite depth of the tank, which influence on results, as shown in the following discussion, seems negligible. Based on these considerations, table 1 summarizes the

appropriate boundary conditions. A set of different analyses have been carried to identify the

Table 1: Boundary conditions for the mesh-based code

	Pressure	Velocity	α
Wedge	$fixedFluxPressure$	$noslip$	$\frac{\partial \alpha}{\partial n} = 0$
Top	$p = 0$	$\frac{\partial U}{\partial n} = 0$	$\frac{\partial \alpha}{\partial n} = 0$
Symmetry	$symmetry$	$symmetry$	$symmetry$
Side	$p = 0$	$\frac{\partial U}{\partial n} = 0$	$\frac{\partial \alpha}{\partial n} = 0$
Bottom	$\frac{\partial p}{\partial n} = 0$	$\frac{\partial U}{\partial n} = 0$	$\frac{\partial \alpha}{\partial n} = 0$

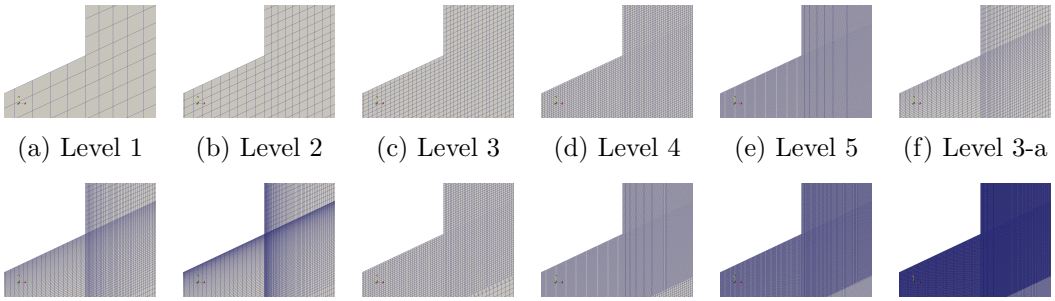

(a) Level 1 (b) Level 2 (c) Level 3 (d) Level 4 (e) Level 5 (f) Level 3-a

(g) Level 3-b (h) Level 3-c (i) Level 2-R1 (j) Level 2-R2 (k) Level 2-R3 (l) Level 2-R4

Figure 3: Details of the various meshes used for RANS sensitivity analysis.

more suitable numerical parameters of the model. In particular two aspects have been investigated: the influence of the simulation time step (i.e. maximum allowable Courant number) and the mesh size. The first analyzed aspect is the influence of the simulations time step. Due to the shock nature of the problem, an adaptive time-step approach has been preferred. This method saves time during the smooth part of the motion (as the initial free falling in air of the wedge) where longer time intervals can be adopted, without affecting any aspects of the solution; switching to smaller time steps when the impact occurs to ensure time accurate calculations of the unsteadiness and of the interaction with water. The selection of the time-step is driven by the maximum allowable Courant number, which has a strong correlation with local flow velocities and to the smaller cell size inside the domain. Starting from a reference mesh arrangement (Level 2 of figure 3), five different Courant numbers have been considered, ranging from 5 to 0.1. As expected, when a Courant number higher than the unity is considered, the solution becomes unstable. On the contrary, as reported in figure 4, the other time selections give qualitatively the same results in terms of maximum pressure peaks (figure 4a) and global forces (figure 4b), even if the computational effort increases of one order of magnitude. These results show that the time-step selection is driven only by the stability constraint, therefore for further simulations a Courant number equal to 0.5 was selected.

The second addressed aspect concerns the mesh size. Three refinements approaches have been

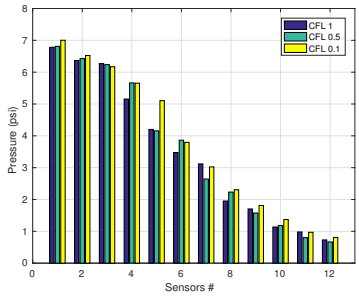

(a) Maximum pressure peaks

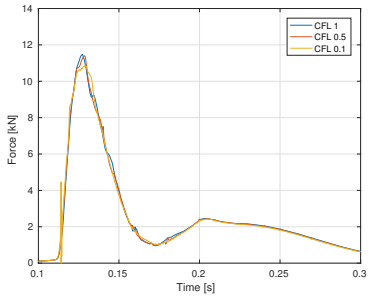

(b) Force time histories for unit of depth

Figure 4: Results variing the Courant number

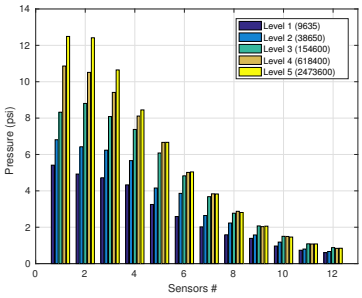

(a) Maximum pressure peaks

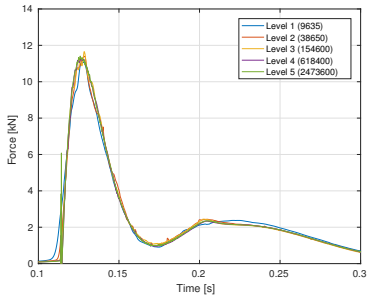

(b) Force time histories for unit of depth

Figure 5: Results variing the global mesh density

considered. At first, a global refinement has been performed halving each time the mesh edges, therefore increasing the number of cells by four times (2-D case). In figure 5 the results for the different meshes, starting from the coarser (with only 9635 cells) up to the finer (with 2.47M cells), are reported. The recorded force signals (figure 5b) are almost equal, except in correspondence to the first impact. In this interval the coarser meshes, due to the free surface smearing, undergoes a slower and anticipated increment of force. These results, however, demonstrate the negligible influence of the mesh size on the global force experienced by the wedge. A completely different conclusion is observed for what regards the pressure peaks on the wedge surface. Figure 5a shows a comparison of the maximum recorded pressure for each sensor. It is clear that even if a very fine mesh has been adopted, the mesh independence has not been reached.

Based on these initial results, different refinement approaches have been proposed. In particular, cells have been clustered in correspondence of the wall boundary layer, using higher mesh gradings in the wall normal direction. This technique does not significantly affect the total cell count by adding cells only locally. Therefore the refinements (namely -a, -b, -c) have been considered starting form the mesh named Level 3. Figure 6a summarizes the results. Again a strong dependence of the pressure intensity by the near wall mesh size has been found, especially in correspondence of the first five pressure probes. Even if this method seems to be able to perform

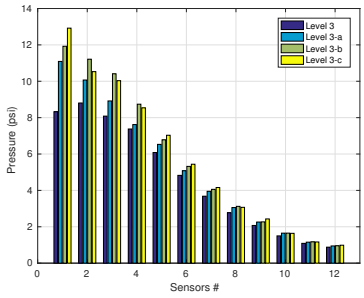

(a) Anisotroping wall refinements

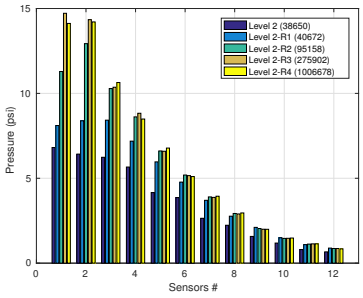

(b) Isotroping wall refinements

Figure 6: Maximum pressure peaks for different near-wall mesh refinements strategies

more accurate calculations with a small increment of computational costs, the selected refinement approach (which refine the cell only in one direction) produces cells with highly aspect ratio which may impair the robustness of the analysis. In particular, this could pose no-negligible issues on the solution stability, especially if further refinements are requested. The final set of refinements has been adopted to overcome this problem. It consists on a recursive isotropic halving of the cells localized only in correspondence of the wall boundary, therefore generating a high quality mesh, in terms of aspect ratio, with a lower impact on the total cell count. Starting form the Level 2 mesh, four refined configurations (namely -R1, -R2, -R3 and -R4) have been arranged. The finer mesh (Level 2-R4) consists of about 1M cells and grants, at the wall, a first cell prism height that is a quarter of the cell size achieved with the global refinements (Level 5 with about 2.47M cells). With this refinement strategy, a certain grid independence is achieved: pressures from meshes Level 2-R3 and Level 2-R4 are very similarly predicted, also in correspondence to the first probes that showed, in the previous analyses, the highest sensitivity to mesh variations. In conclusion, if the focus is on local pressure distribution on the wedge surface, an enough finer mesh near the wall should be used, taking care of the mesh quality. For the present test case a squared near wall cell with edges of 0.8mm (Level 2-R3, 275k cells) can be considered as a good compromise. On the contrary, if the focus is only on the prediction of global force exerted by the wedge, a regular mesh without the local, isotropic refinements at wall (Level 2, 38k cells) with the edge length of 13mm, ensures sufficient accuracy.

As previously reported all the sensitivity analyses have been carried out imposing the wedge motion extracted by the original paper. Afterwards, the final mesh setup (Level 2-R3) has been used to perform a free-falling simulation where the vertical motion has been solved at each time-step. In figure 7a the pressure peaks from the numerical simulations (imposing or solving the motion) are compared with the experimental measurements. In parallel, also the experimental and the computed motion are shown in figure 7b. The two numerical simulations differ both in terms of pressure peaks and motion. The motion discrepancies, which are directly connected also with the pressure differences, can be due to the difficulties in extracting the measured law of motion that is given, in [17], only graphically. Anyway, non negligible differences with the experimental data are highlighted in terms of pressure behavior, even if the global peak is quite in good agreement with the measured one (lower than 5%). This last discrepancy can be partially

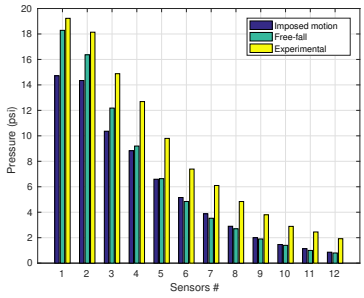

(a) Maximum pressure peaks

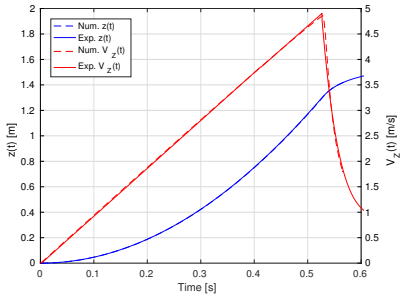

(b) Position and Velocity laws

Figure 7: Comparison of the imposed falling law and the free falling simulations with experimental measurements

justified by the 2-D simplification adopted for all the numerical simulations. Infect, neglecting the border effect in span-wise direction, a higher total force should be computed in the computation, which consequently make the wedge penetration velocity lower. On the contrary this border effect can be considered negligible related to the pressures experimentally recorded in the center line of the wedge. As previously reported by [3], [18], [19], the velocity penetration is directly connected with the pressure peak behavior and intensity.

3.2 MESH-LESS APPROACH: SPH

An open-source SPH solver [20] originally formulated by [21] has been selected for the proposed analysis. It is specifically designed to exploit GP-GPU computation allowing for relatively fast computations using a great number of particles (depending of course on the GPU hardware installed).
According to the SPH method, the equations of the fluid dynamics are solved by a mesh-free Lagrangian approach based on particles description. Each particle carries all the relevant field information and is used for the numerical integration of the *PDEs* for the mass and momentum conservation. The *kernel approximation* involves the representation of a field variable (e.g. V, ρ or p) and its derivatives in a continuous integral form by a suitable kernel function; the *particle approximation* step refers to the discretization process of the computational domain that is redefined by an initial distribution of discrete particles; according to this discrete model, field variables on a particle are computed by approximation using the nearest neighbor particles.
Giving a function $f(x)$ its integral form is expressed according to Eq. (3):

$$f(x) = \int_{\Omega} f(x')\delta(x - x')dx' \tag{3}$$

Using a kernel function $W(x - x', h)$ that depends on the so-called smoothing length h, Eq. (3) can be written in terms of Kernel approximation as in Eq. (4); this kernel, that ideally would be a Dirac function, is substituted by some analytic formulations that in any case vanish for separations greater than kh. A cubic spline kernel function (Eq. (5)) is selected for the present

analysis.

$$\langle f(x)\rangle = \int_{\Omega} f(x')W(x-x',h)dx' \tag{4}$$

$$W(r,h) = \frac{7}{4\pi h^2}\begin{cases}\frac{3}{2}q^2+\frac{3}{4}q^3 & 0\le q\le 1\\ \frac{1}{4}(2-q)^3 & 1\le q\le 2\\ 0 & q\ge 2\end{cases} \tag{5}$$

Even if water is an incompressible fluid, assuming it is weakly compressible allows for pressure computation from the state equation (Eq. (6)) instead of solving for the Poisson's equation.

$$p = \frac{c_0^2\rho_0}{\gamma}\left[\left(\frac{\rho}{\rho_0}\right)^{\gamma}-1\right] \tag{6}$$

In Eq. (6), c_0 is the sound speed ranging from 50 m/s up to 250 m/s to ensure $Mach < 0.1$ and γ is a constant assumed equal to 7.
According to the SPH formulation, both the mass and the momentum conservation laws, Eq. (7) and Eq. (8) respectively, are written in terms of particles approximation as follows:

$$\frac{d\rho_i}{dt} = \sum_{ij} m_j\left(u_i-u_j\right)\nabla_i W_{ij} \tag{7}$$

$$\frac{d\mathbf{u}_i}{dt} = -\sum_{ij} m_j\left(\frac{P_i}{\rho_i^2}-\frac{P_j}{\rho_j^2}+\Pi_{ij}\right)\nabla_i W_{ij} + g \tag{8}$$

The summation over the two indexes i and j accounts for particles interactions; m, u and P are the particle mass, velocity and the pressure at a particle respectively. Π_{ij} is a force contribution used to avoid tensile instabilities, defined according to the following (9):

$$\Pi_{ij} = \begin{cases}\frac{\alpha\mu_{ij}\bar{c}_{ij}}{\rho_{ij}} & u_{ij}r_{ij} < 0\\ 0 & u_{ij}r_{ij} > 0\end{cases} \tag{9}$$

being the artificial viscosity coefficient α the main parameter that controls this additional force term.
First a preliminary analysis has been carried out in order to select the most suitable dimensions of the computational domain that needs to be modified with respect to the physical domain used for the experiments to cut off possible reflections of the pressure waves propagating in the fluid. A 2D tank $6m$ wide and filled for $3m$ depth has been used. The four significant parameters of the SPH model listed in Table 2 have been considered for the proposed systematic analysis. The possible values assigned to each of them have been selected based on the suggested values for such a class of problems. The peak pressures measured at the twelve probe locations and the time-histories of the total vertical forces on the wedge are shown in Figures 8, 9, 10, 11 and 12 for CFL, C_S, d_P, α and C_{Sound} variations respectively. The global forces prediction is generally more stable with respect to parameter variations, being the oscillations of the peaks always close to $13kN$, occurring in a time lapse of $^2/_{100}s$. The peak pressure computation rises more issues; its

Table 2: SPH model parameters and ranges used in the systematic analysis.

Parameter	Values
CFL	[0.1; 0.2; 0.5]
C_S	[0.8; 1.0; 1.2]
d_P	[$1.0e^{-03}$; $1.5e^{-03}$; $2.0e^{-03}$]
α	[0.01; 0.05; 0.10]
C_{Sound}	[20; 25; 30]

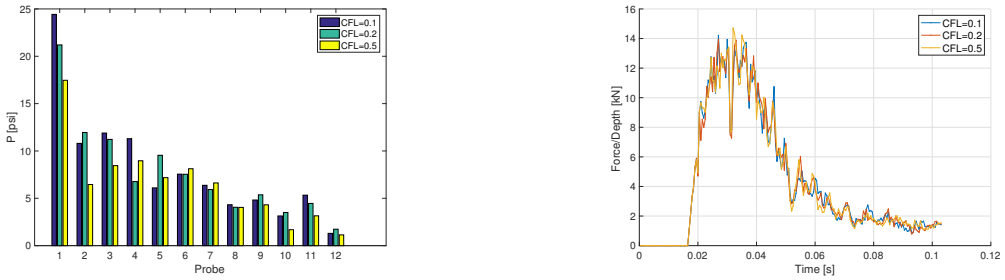

(a) Pressures (b) Forces

Figure 8: Peak pressures (left) and global vertical forces on the wedge (right) with respect to variations of the *Courant-Friedrichs-Lewy* number CLF.

trend over the twelve probes is computed fairly well, i.e. decreasing from the cusp of the wedge to its knuckle; however, analyzing parameter variations effects on each probe separately no clear trends can be identified. Figure 13 is used to further check on this unstable behavior found on the measured (local) variables; three runs of the same SPH configuration have been performed and pressure time histories at the probe n.3 have been recorded at two different distances from the wedge face, namely at $d/h = 1.5$ and $d/h = 2.0$. For both d/h values the three records show different peaks of the pressures and even slightly different time series. This behavior of the SPH solver in predicting very local variables should be further analyzed to better understand the reasons and eventually to provide a quantification of the related uncertainty.

4 URANS AND SPH SOLUTIONS COMPARISON

The two numerical solutions have been finally compared in the case of the experimental drop test performed by [17]. Results in terms of wedge vertical displacement $z(t)$ and drop speed $V_Z(t)$ are shown in Figure 14a while vertical force comparison is shown in Figure 14b. A very good agreement of both numerical solutions with the measured values of displacement and drop speed is found, confirming that the dynamics of this class of problems is well captured consistently with the results shown in the sensitivity analysis with respect to the global forces. This general agreement is also revealed by the qualitative comparison of the free surface of the two methods shown in Figure 15 at three time steps during the drop; the position of the pile-up

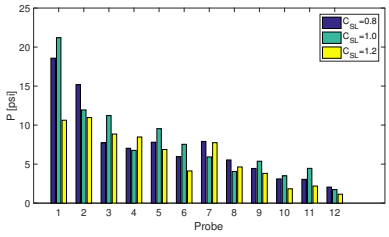

(a) Pressures

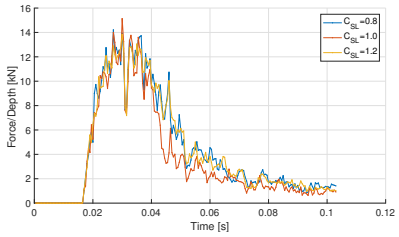

(b) Forces

Figure 9: Peak pressures (left) and global vertical forces on the wedge (right) with respect to variations of the smoothing length coefficient C_S.

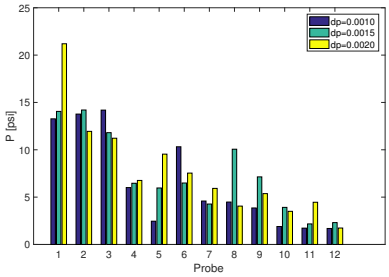

(a) Pressures

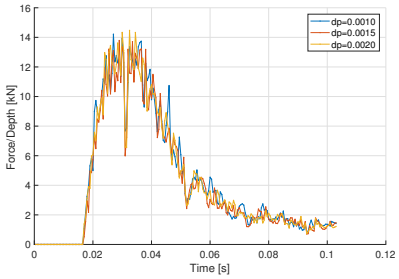

(b) Forces

Figure 10: Peak pressures (left) and global vertical forces on the wedge (right) with respect to variations of the particles resolution d_P.

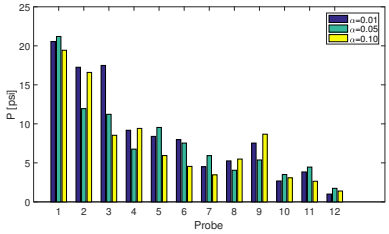

(a) Pressures

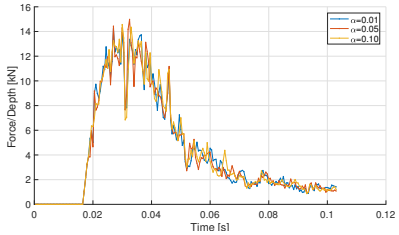

(b) Forces

Figure 11: Peak pressures (left) and global vertical forces on the wedge (right) with respect to variations of the artificial viscosity coefficient α.

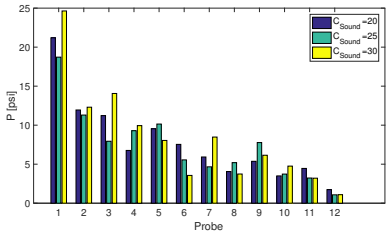

(a) Pressures

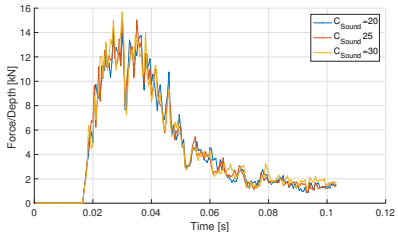

(b) Forces

Figure 12: Peak pressures (left) and global vertical forces on the wedge (right) with respect to variations of the sound coefficient C_{Sound}.

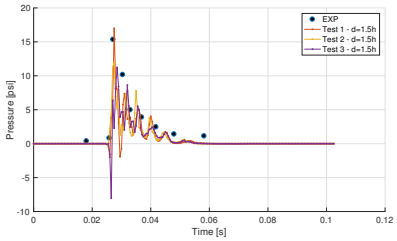

(a) $^{d}/_{h} = 1.5$

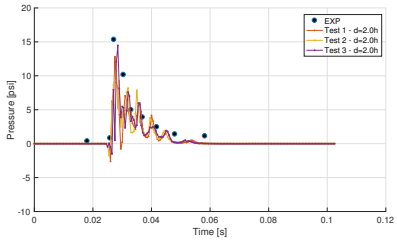

(b) $^{d}/_{h} = 2.0$

Figure 13: Pressure time-history for the Probe n.3. Experimental measurements shown by black dots. Three runs of the same SPH configuration are shown by red, yellow and violet curves. Pressure probes placed at distance over smoothing length ratios of $^{d}/_{h} = 1.5$ (left) and of $^{d}/_{h} = 2.0$ (right) from the wedge border.

is well captured by both solutions while the water jet appears to be more unstable in the SPH compared to the URANS one. The vertical force agreement is again satisfactory: both the force peak and the global trend are consistent between the URANS and the SPH solutions. This final comparison, although limited to a single test, provide a basis for the practical use of both methods for the numerical prediction of such a class of hydrodynamics problems.

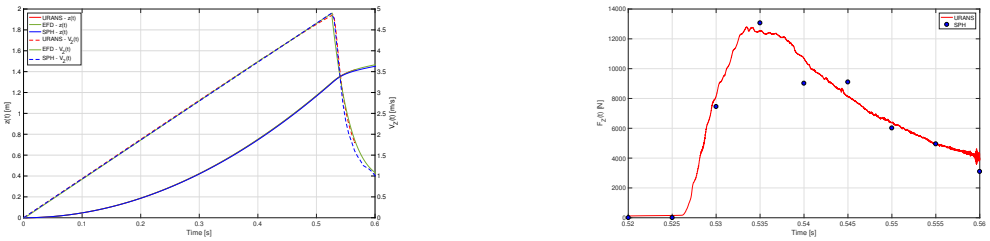

(a) $z(t); V_Z(t)$ (b) $F_Z(t)$

Figure 14: Wedge drop test (free falling), $h_{Drop} = 1.3m$, $M_{Wedge} = 94kg$. Comparison of the URANS and SPH solutions. Figure 14a: wedge displacement (solid curves) and wedge vertical velocity (dashed curves). Experimental results in green, URANS results in red and SPH results in blue. Figure 14b: wedge total vertical force. URANS results are shown by solid red curve; SPH resutls are shown by blue dots.

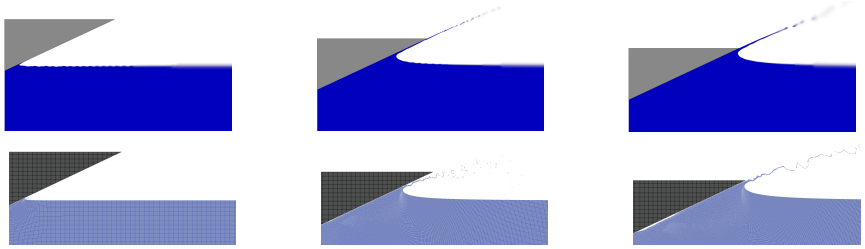

(a) t=0.524 s (b) t=0.564 s (c) t=0.604 s

Figure 15: Comparison of free surface elevation at three times during the simulations. RANS on the upper row. SPH on the lower row.

5 CONCLUSIONS

The problem of numerical modeling of 2D wedge impact hydrodynamics by mesh-based and mesh-less approaches has been addressed in this study, focusing on the effect of systematic variations of the simulation set-up on the results. Open source solvers have been used for both numerical techniques: *OpenFOAM* libraries have been selected to achieve the RANS solution while *DualSHPysics* has been chosen as SPH solver. Both global and local responses have been analyzed, i.e. the total vertical force on the wedge and the peak pressures on twelve measurement probes along the side of the edge respectively. Numerical predictions have been compared to

experimental measurements on a 25° wedge for which both the displacement and the pressures time histories were available.
Analyzing the results two conclusions valid for both approaches can be derived: (a) the prediction of the global forces is generally stable, i.e. not really affected by model parameter variations, consequently also the prediction of the vertical motion, and (b) the prediction of the peak pressure during the impact strongly depends on the simulation set-up. Considering the mesh-based RANS technique it is possible to find a clear trend of the local responses (the pressures) when model parameters are changed; the convergence is found but at the cost of increasing the computational effort. The sensitivity analysis on the SPH solution on the other hand reveals that the evaluation of the pressure peaks is not as robust as the prediction of the global vertical forces. The free falling drop test however shows that both solutions provide a reasonably good agreement compared to the experimental measures and are consistent in terms of force prediction.

REFERENCES

[1] Von Karman, T. *The impact on seaplane floats during landing.* Technical Notes, National Advisory Committee for Aeronautics (1929).

[2] Wagner, H. *Phenomena associated with impacts and sliding on liquid surfaces.* Z. Angew. Math. Mech. (NACA Library, Langley Aeronautical Laboratory), Vol. 12(4), pp. 193-215 (1932).

[3] Dobrovolskaya, Z.N. *On some problems of similarity flow of fluid with a free surface.* Journal of Fluid Mechanics, Vol. 36(4), (1969).

[4] Zhao, R., Faltinsen, O. *Water entry of two-dimensional bodies.* Journal of Fluid Mechanics, Vol. 246, pp. 593-612, (1993).

[5] Sun, H., Faltinsen, O. M. *Water impact of horizontal circular cylinders and cylindrical shells.* Applied Ocean Research, Vol. 28(5), pp. 299-311, (2006).

[6] Faltinsen, O.M. *Water Entry of a Wedge with Finite Deadrise Angle.* Journal of Ship Research, Vol. 46, No. 1, March 2002, pp. 3951, (2002).

[7] Shadloo, M.S., Oger, G., Le Touze, D. *Smoothed particle hydrodynamics method for fluid flows, towards industrial applications: Motivations, current state, and challenges.* Computers and Fluids, Vol. 136, pp. 1134, (2016).

[8] Oger, G., Doring, M., Alessandrini, B., Ferrant, P. *Two-dimensional SPH simulations of wedge water entries.* Journal of Computational Physics, Vol. 213, pp. 803822, (2006).

[9] Muzaferija, S., Peric, M. *Application of a two-fluid finite volume method to ship slamming.* Journal of Offshore Mechanics and Arctic Engineering, Vol. 121, pp. 47, (1999).

[10] Veen, D. J., Gourlay, T. P. *SPH study of high speed ship slamming.* In 3rd ERCOFTAC SPHERIC Workshop on SPH Applications, Lausanne, Switzerland, pp. 4-6, (2008).

[11] Viviani, M., Brizzolara, S., Savio, L. *Evaluation of slamming loads using smoothed particle hydrodynamics and Reynolds-averaged NavierStokes methods.* Proceedings of the Institution of Mechanical Engineers, Part M: Journal of Engineering for the Maritime Environment, Vol. 223(1), pp. 17-32, (2009).

[12] Marcer, R., Berhault, C., de Jouette, C., Moirod, N., Shen, L. *Validation of CFD codes for slamming.* In Proceedings of the European Conference on Computational Fluid Dynamics (ECCOMAS CFD10), pp. 14-17, (2010).

[13] Brizzolara, S., Villa, D., Gazzola, T., Tryaskin, N., Moirod, N., De Lauzon, J., Diebold, L. *Influence of Raised Invar Edges on Sloshing Impact Pressures-Numerical Investigations.* In Proceedings of 3rd International Conference on Marine Structures (MASTRUCT2011), Hamburg, Germany, pp. 3-8, (2011).

[14] Farsi, M., Ghadimi, P. *Simulation of 2D symmetry and asymmetry wedge water entry by smoothed particle hydrodynamics method.* Journal of the Brazilian Society of Mechanical Sciences and Engineering, Vol. 37(3), pp. 821-835, (2015).

[15] Farsi, M., Ghadimi, P. *Finding the best combination of numerical schemes for 2D SPH simulation of wedge water entry for a wide range of deadrise angles.* International Journal of Naval Architecture and Ocean Engineering, Vol. 6(3), pp. 638-651, (2014).

[16] Sasson, M., Chai, S., Beck, G., Jin, Y., Rafieshahraki, J. *A comparison between Smoothed-Particle Hydrodynamics and RANS Volume of Fluid method in modelling slamming.* Journal of Ocean Engineering and Science, Vol. 1, pp. 119128, (2016).

[17] Yettou, E.M., Desrochers, A., Champoux, Y. *Experimental study on the water impact of a symmetrical wedge.* Fluid Dynamics Research, Vol. 38(1), pp. 46-66 (2006).

[18] Mei, X. *On the impact of arbitrary two-dimensional sections.* Masters Thesis, Department of Ocean Engineering, MIT,Cambridge, MA. (1998).

[19] Mei, X., Lui, Y., Yue, D.K.P. *On the water impact of general two-dimensional sections.* Applied Ocean Research 21.(1999).

[20] Gomez-Gesteira, M., Rogers, B.D., Crespo, A.J.C., Dalrymple, R.A., Narayanaswamy, M. and Dominguez, J. M. *SPHysics–development of a free-surface fluid solver–Part 1: Theory and formulations.* Computers & Geosciences, Vol. 48, (2012).

[21] Monaghan, J.J. *Smoothed particle hydrodynamics.* Annual Review of Astronomy and Astrophysics, Vol. 30, pp. 543-574 (1992).